

Microgravity Mass Gauging with Capacitance Sensing: Sensor Design and Experiment

Matthew A. Charleston^{1*}, Shah M. Chowdhury¹, Qussai M. Marashdeh¹, Benjamin J. Straiton¹,
Fernando L. Teixeira²

¹Tech4Imaging, LLC; ²The Ohio State University

Abstract: *The use of capacitance sensors for fuel mass gauging has been in consideration since the early days of manned space flight. However, certain difficulties arise when considering tanks in microgravity environments. Surface tension effects lead to fluid wetting of the interior surface of the tank, leaving large interior voids, while thrust/settling effects can lead to dispersed two-phase mixtures. With the exception of Electrical Capacitance Volume Tomography (ECVT), few sensing technologies are well suited for measuring annular, stratified, and dispersed fluid configurations as well as handling the additional complications of mechanical installation inside a spherical tank. To optimize the design of future ECVT based spherical tank mass gauging sensors, different electrode plate layouts are considered, and their effect on the performance of the sensor as a fuel mass gauge is analyzed through the use of imaging and averaging techniques.*

Keywords: Electrical Capacitance Volume Tomography, Microgravity Mass Gauging, Capacitance, Propellant, Sensor

1. Introduction & Background

Propellant mass gauging has long been a critical measurement in rocketry. Although a simple level measurement problem on the ground, mass gauging in microgravity is a complex challenge. In a low-gravity environment, surface tension effects distort the liquid/gas phase interface, and momentum effects can create dispersed fluid configurations [1]. Liquid level sensing modalities like ullage pressure correlations, ultrasonic interface detection, or coaxial capacitance probes have been used in a number of flights but require wasteful settling thrusts to generate an accurate measurement [2]. Other established methods such as propellant mass flow integration, or bookkeeping, are only applicable when thrusting, accumulate error over time, and are unable to detect propellant leaks [1]. The PVT method, based on adding a pressurizing gas and using the ideal gas law, can gauge propellant mass but loses accuracy as the amount of fluid in the tank decreases [3]. Thermal propellant gauging, on the other hand, increases in accuracy at low fill levels but makes assumptions on fluid position. Radio frequency and acoustic modal gauging methods are under development but require detailed understanding of the fluid configuration [4] [5]. Despite decades of research, microgravity propellant mass gauging remains an unsolved problem and is an active area of focus for NASA [6]. A new, on-demand, passive measurement technique that is accurate irrespective of fluid configuration is clearly needed for future orbital and interplanetary missions. [7]

*Corresponding Author: m.charleston@tech4imaging.com 1910 Crown Park Ct, Columbus, OH 43235
This work was performed with support from NASA contract 80KSC022PA006

Electrical Capacitance Tomography (ECT) has an extensive history of use as a sensing modality for multiphase flows [8]. It has a number of advantages over other tomographic techniques including high speed acquisition, no harmful radiation, non-intrusive construction, and ability to withstand high temperatures and pressures [8] [9]. Electrical Capacitance Volume Tomography (ECVT) is a more recently developed technique that collects measurements across an entire three-dimensional volume instead of one or more two-dimensional planes. ECT and ECVT have similar primary applications including fluidized beds, oil concentration measurement, pneumatic conveyance, and various other multiphase flow applications [10]. In ECVT sensors, an electrode or plate is individually excited while an electric current from every other plate is measured. The measurement process is repeated sequentially until all plates are excited. Using this strategy, the number of independent measurements, or “sensing channels”, M , is given in terms of the number of plates, N , in Equation 1. [8] [11]

$$M = \frac{N(N-1)}{2}$$

Equation 1

Capacitance-based fuel mass gauging has seen substantial scientific interest. In the 1960s, Capacitance level sensing probes were implemented on the Saturn V and an ECT-like whole tank capacitance gauge was tested [1]. Recently, ECVT mass gauging has emerged as a promising method for microgravity propellant measurement. Several teams have investigated the accuracy of ECVT sensors in microgravity [12] [13] [14] [15] including during sloshing conditions [16]. These studies, however, did not systematically analyze or improve the sensor design.

2. Sensor Design

The term “ECVT sensor” and similar terms are used throughout this paper to describe a sensor designed to collect volumetric capacitance data for the purpose of fluid mass gauging. The use of tomographic reconstruction techniques to create an ECVT image is not necessarily the most accurate method to measure the fluid mass and as such, different algorithms using the same ECVT capable sensor are explored to assess the effectiveness of various techniques.

The principal concerns when designing an ECVT mass gauge are dynamic range, signal to noise ratio (SNR), imaging resolution, design complexity, and signal linearity with volume fraction. The dynamic range of the sensor is the measurable difference in signal magnitude between the 2 phases present in the region. For a typical 2 phase liquid/air measurement, the dynamic range is evaluated as the signal difference between a sensor filled with air and filled with liquid. The SNR for each channel is the ratio of the dynamic range of the sensor to the noise in the measurement signal, typically represented in decibels. It is calculated according to Equation 2 where n is each channel.

$$SNR_n = 20 \log_{10} \left(\frac{C_{n,full} - C_{n,Empty}}{STD(C_{n,full})} \right)$$

Equation 2

When comparing sensor performance in measuring volume fraction, a sensor dynamic range and sensor SNR are calculated by averaging the dynamic range and SNR of the channels. The factors that influence dynamic range and SNR are largely the same, large electrode plate areas, close proximity, and parallel

geometry lead to high dynamic range and high SNR [10]. Optimizing these parameters, however, results in a reduction of other performance parameters in response.

Imaging resolution can be hard to quantify for ECVT applications, as soft field tomography can resolve objects differently based on the reconstruction technique used to generate images. Furthermore, the imaging resolution changes with different flow patterns or regimes. Generally, increasing the number of electrodes, and therefore the number of independent measurements, increases the spatial resolution in the reconstructed image [11, 17]. However, for fixed volume containers, an increase in electrode count must be accompanied by a corresponding decrease in electrode area, typically decreasing dynamic range and SNR.

Increasing the electrode count can also increase the number of non-adjacent plates. An adjacent plate pair has a high mutual capacitance, but the sensitivity is strongly biased towards the common plate edge and away from the center [8]. Non-adjacent plates have a higher dynamic range, SNR, and linearity than adjacent plates and the number of non-adjacent plates is therefore one of the most important parameters to optimize.

Signal linearity with respect to fluid volume fraction has a strong effect on the accuracy of the overall sensor. The interfaces between plates cause singularities in the sensitivity of the electrodes, that is, when the fluid boundary passes a plate boundary the measured signal change is not proportional to the volume fraction change. Poor signal linearity leads to effects such as the measured volume fraction for a constant volume of liquid changing as the sensor rotates in a gravity field. Signal non-linearity is combated by increasing the number of electrode plates and averaging signals together to calculate volume fraction. This increases the number of singularities but evenly disperses them around the sensing region to smooth their effect on the averaged signal.

The design complexity of ECVT sensors is of paramount importance to the ultimate commercial implementation of the solution. A high number of plates leads to many cables, tank/vessel liquid tight penetrations, mechanical joints, etc. All serving to increase the risk of a manufacturing defect or failure in the field.

The individual design parameters and their effects discussed here are summarized in Table 1 and are often at odds with one another. Therefore, an ECVT tank designer must strive to balance signal strength, resolution, accuracy, and complexity when building a system.

General Effect of an Increase in Design Parameters					
Design Parameter	Design Complexity	Dynamic Range	SNR	Imaging Resolution	Signal Linearity
Number of Plates	↑	↓	↓	↑	↑
Gap Between Plates	No Effect	↓ ¹	↓	↓	↑
Rotational Order	↑	No Effect	No Effect	No Effect	↑
Number of Non-Adjacent Plates	↑	↑	↑	↑	↑

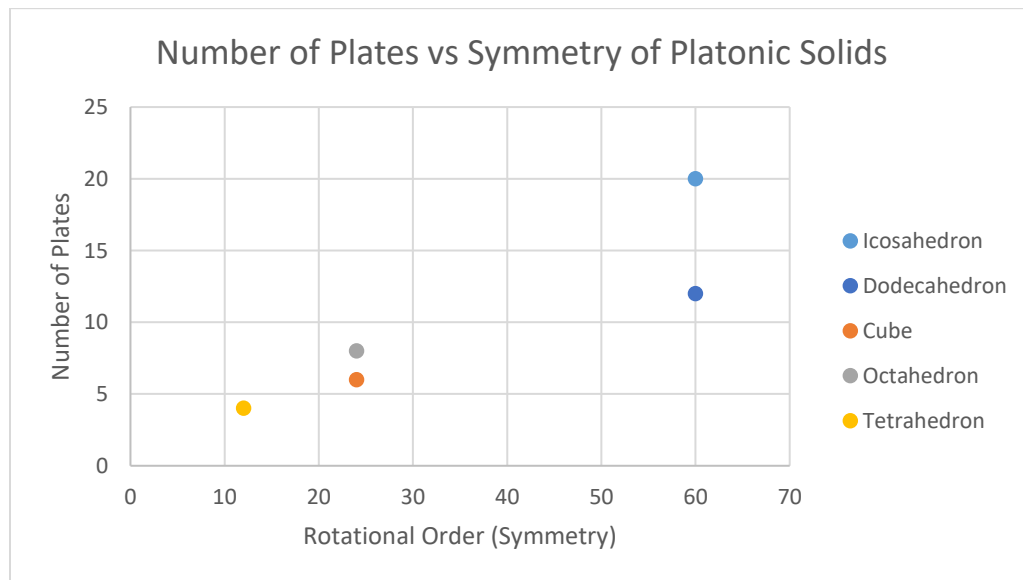
¹ A sensor design with only adjacent pairs may be an exception to this guideline, where increasing the gap can increase the dynamic range by increasing the parallelism of the plates.

Table 1: ECVT Design Parameters

In traditional cylindrical ECT and ECVT sensors, the electrodes are typically a tessellation of rectangles. Other tessellations of polygons such as triangles have been tested [18]. Electrode geometry consisting of regular polygons is ideal in ECVT sensors because it results in an axially/radially equal sensitivity strength distribution, improving image reconstruction and regularization [18].

When imaging a spherical region, different electrode geometry must be considered, as planar tessellations do not have the same advantages when projected in the spherical plane. Gut [13] tested a design with 24 electrodes consisting of 3 rows of 8 rectangular plates arrayed around a cylinder and then projected onto a sphere. This projected pattern has irregular polygons, and the uneven sensitivity distribution resulted in errors in the calculated volume fraction that varied significantly with rotation of the tank. An even sensitivity distribution is essential because an uneven distribution causes different fluid mass to be measured when the fluid orientation changes. In order to smooth the sensitivity distribution, geometry that tessellates onto a sphere must be used, and regular tessellations are preferred. Regular tessellations utilize the whole surface area with the most symmetry. There are a finite number of regular polyhedra that can be projected onto a sphere. These are known from antiquity and referred to as platonic solids [19].

	Vertices	Plates	ECVT Channels	Non-Adjacent Channels	Rotational Order
Tetrahedron	4	4	6	0	12
Cube	8	6	15	3	24
Octahedron	6	8	28	4	24
Dodecahedron	20	12	66	36	60
Icosahedron	12	20	190	100	60

Table 2: Relevant Properties of Spherical Projections of Platonic Solids*Figure 1: Number of Plates vs Rotational Symmetry for Platonic Solids*

Selecting a projection of a platonic solid ensures an even sensitivity distribution and the efficient utilization of the entire surface area of the sphere. What remains is selecting the specific platonic solid to optimize the properties in Table 1, Design Complexity, Dynamic Range, SNR, Imaging Resolution, and Signal Linearity for the specific application. The relevant properties for each platonic solid are laid out in Table 2. Figure 1 elucidates the relative advantage of designs based on their rotational symmetry and the number of electrode plates. A Tetrahedron would make a bad ECVT sensor as it has only adjacent plates, and therefore would have poor sensitivity in the center. A cube may make a good ECVT sensor as it has three non-adjacent channels and is more rotationally symmetric. However, the cube shape is hard to physically construct inside a sphere as it is difficult to manufacture and separate the sensor into halves. The octahedron is much easier to construct than the cube, having a clear equator. It has four non-adjacent channels and additionally four semi-adjacent channels that only share a vertex and not an entire edge. This makes it a good candidate for study. The dodecahedron is highly rotationally symmetric and has a large number of non-adjacent channels. Although it does not have a clear equator, the equatorial plates can be mounted to each hemisphere as seen in Figure 3. Finally, the icosahedron has a much better imaging resolution due to a dramatically higher number of channels. It is also highly rotationally symmetric and has many non-adjacent plates. However, the large number of plates and channels means that the sensor would be difficult to construct and would require more intense post-processing before a volume fraction measurement could be generated. This study focuses on the octahedron and the dodecahedron designs, selected to maximize plate area, signal linearity, and SNR.

3. Construction

The first intuitive design is a spherical projection of an octahedron. This is a natural first design because it has polar vertices for fluid filling and draining and has an equatorial gap that allows the separation of the two hemispheres for easy assembly and maintenance. There are only 8 total plates, and each plate touches a pole, allowing the signal cables to enter and exit the sphere neatly at the poles.

The second design is a spherical projection of a dodecahedron. This design has several advantages over the first design. The singularities at each of the vertices are more evenly distributed, and the higher symmetry improves the signal linearity with fluid distribution. Due to the increased number of channels, better imaging resolution is achieved, and a more robust overall measurement is generated. The primary advantage, however, is the addition of more plates that do not share a common edge. This permits more sensitive measurement of the interior of the tank, with higher dynamic range.

For both designs, a flanged acrylic hemisphere with an internal diameter of 9.5 inches and a thickness of $\frac{1}{4}$ inch was used as the tank. The outside of the tank was sprayed with a conductive nickel paint to act as a ground shield, and then coated with a scratch resistant paint for protection. A silicone gasket and 16 bolts were used to secure the hemispheres together with a leak tight seal. Four of the 16 bolts were threaded rods to provide feet for the sensor. A hole was drilled in the top and bottom of the sensor. The bottom hole had a liquid tight multi-hole cord grip installed to allow the cables to exit. The top hole was left open for filling and

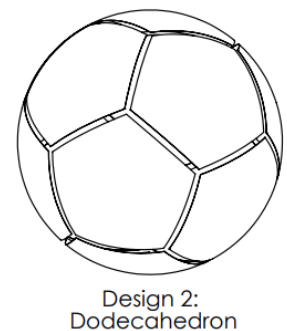
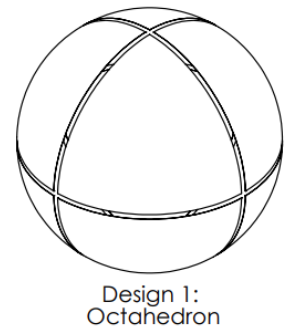
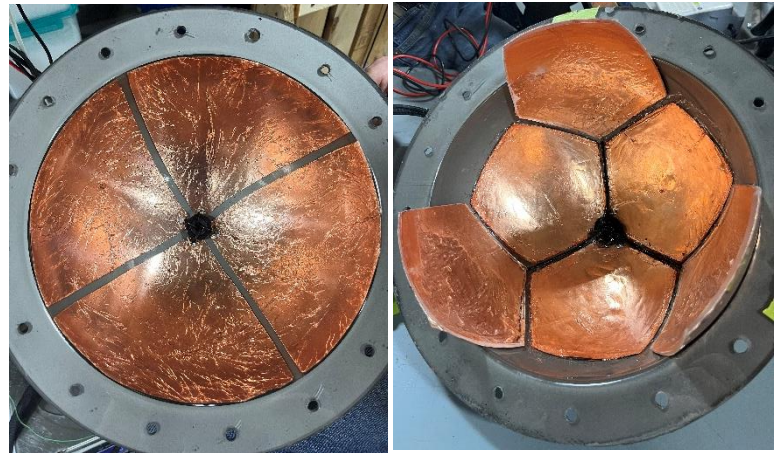


Figure 2: Sensor Plate Configurations

draining of the sensor. A gap of 0.25 inch between the plates was used to maximize plate area. A data acquisition system from Tech4Imaging, LLC was used to collect data for each sensor.

The plates for the first design were made from 0.75 thou thick adhesive backed copper foil. The plates were adhered to the surface of the sensor and $\frac{1}{4}$ inch gaps were cut between them. Solder connections to each plate were made near the poles, the ground shield was terminated 0.5 inch from the plate and the wires were staked with epoxy to prevent movement.

The second design is more complex and requires a different plate construction method. A thicker 0.003 inch copper was selected. It was press-formed in a 3D printed mold to the curvature of the sphere and trimmed to size. The 3 plates near each pole were epoxied into place. The plates near the equator protrude past the edge of the hemisphere and therefore needed support. These plates were epoxied to the outside of curved acrylic plates and then epoxied to the hemisphere, allowing all the copper plates to be on the same radius. The wires for the equatorial plates were routed in between the polar plates back to the poles of the sensor.



Design 1

Design 2

Figure 3: Sensor Construction

4. Experiment

The primary propellants of interest for microgravity gauging are cryogenic liquid oxygen and liquid hydrogen. These materials have very low dielectric constants as shown in Table 3, making them challenging to distinguish from air. A suitable less explosive test analog is needed. Liquid nitrogen has a dielectric constant between hydrogen and oxygen, but operations at cryogenic temperatures require a more robust test fixture, which was not the focus of this study. Special heat transfer fluids like Galden HT-55 have low dielectric constants and have been used in other studies, [12] but at the time of this study were difficult to obtain due to supply issues. A standard mineral oil was ultimately selected because it is safe, readily available, and can be used at room temperature without special equipment. The disadvantage is the higher dielectric constant which will provide a higher signal and potentially more non-linearity than the true propellants.

Material	Dielectric Constant	Temperature (K)
Hydrogen (H ₂) [20]	1.228	20.4
Oxygen (O ₂) [20]	1.507	80
Nitrogen (N ₂) [20]	1.454	70.15
Mineral Oil ²	2.16	296.15
Galden HT-55 [21]	1.86	298.15

Table 3: Dielectric Constants of Relevant Materials

A series of stratified filling experiments illustrated in Figure 5 were conducted to measure the response of the sensors to volume fraction. A sensor was placed on a scale and then repeatedly filled with a discrete amount of mineral oil. At each fill level, a mass reading was recorded along with a 60 second ECVT dataset. Then, to give an indication as to the rotational stability, each sensor was tilted to 45 degrees and the filling repeated. Finally, a 3.94" diameter polypropylene ball filled with oil was advanced from the top to the bottom of the tank in $\frac{1}{4}$ " increments to determine the positional stability of the design.

The sensor and ball position test fixture are shown in Figure 4. A polypropylene rod is attached to the ball and marked with graduations. A clamp is used to suspend the ball at specific heights inside the spherical tank.

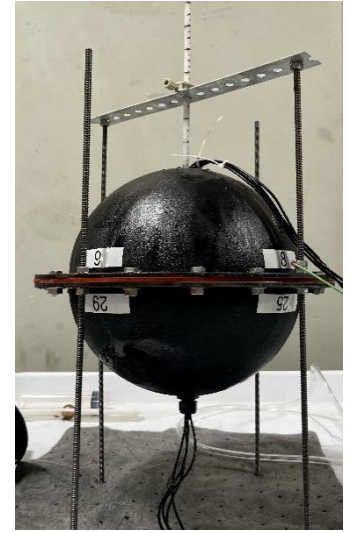


Figure 4: Ball Position Test Fixture

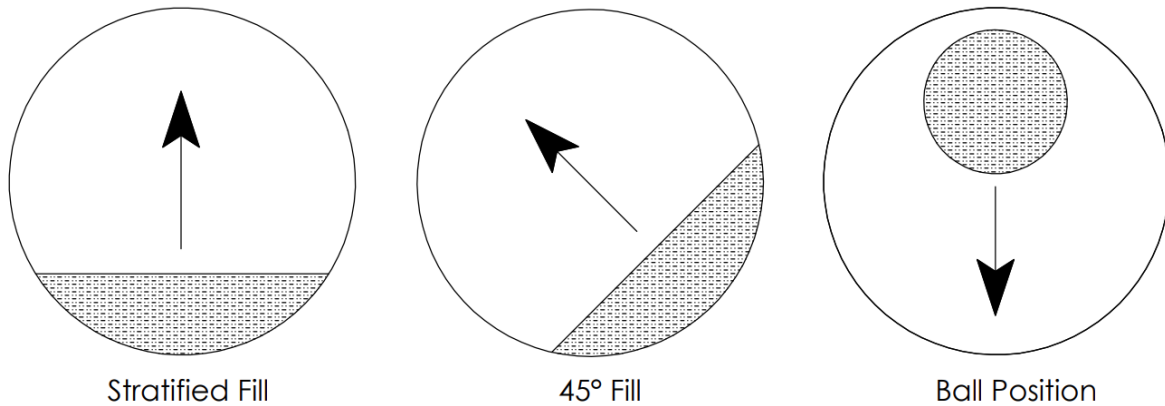


Figure 5: Experiment Tests

The signal gain, dynamic range, and SNR for each measurement channel are naturally different due to small imperfections in the system design. Each channel is therefore normalized between the full and empty measurements to scale the datasets for comparison. The Dynamic Range and SNR are averaged together to provide the Dynamic Range and SNR of the sensor. The collected data was analyzed in three ways, as independent channels, groups of channel types, and as images. Due to the spherical symmetry of the design, there are a finite number of relative plate configurations, as illustrated in Figure 6. Also, in Figure 6 the quantity of each type of plate configuration is listed. The Octahedron Sensor has adjacent plates that share one edge, semi-adjacent plates that share one vertex, and opposite plates that share no edges or vertices. The Dodecahedron has adjacent plates

² Measured in-house using Brookhaven BI-870 Dielectric Constant Sensor

that share one edge, cross plates that share no edges or vertices, and opposite plates that are antipodes. These channel types have similar sensitivity and similar response profiles. The relationships between the channel types can provide important information about the fluid state. A high adjacent to cross channel signal ratio would indicate the fluid is in an annular configuration and a low ratio would indicate a ball of fluid in the middle. Use of these parameters in mass gauging algorithms could improve the accuracy with fluid position. Additionally, the channel types can be treated independently during image reconstruction, reducing the ill-posedness and yielding better results. The channel type images could then be combined into one image, reducing the overall burden of image reconstruction.

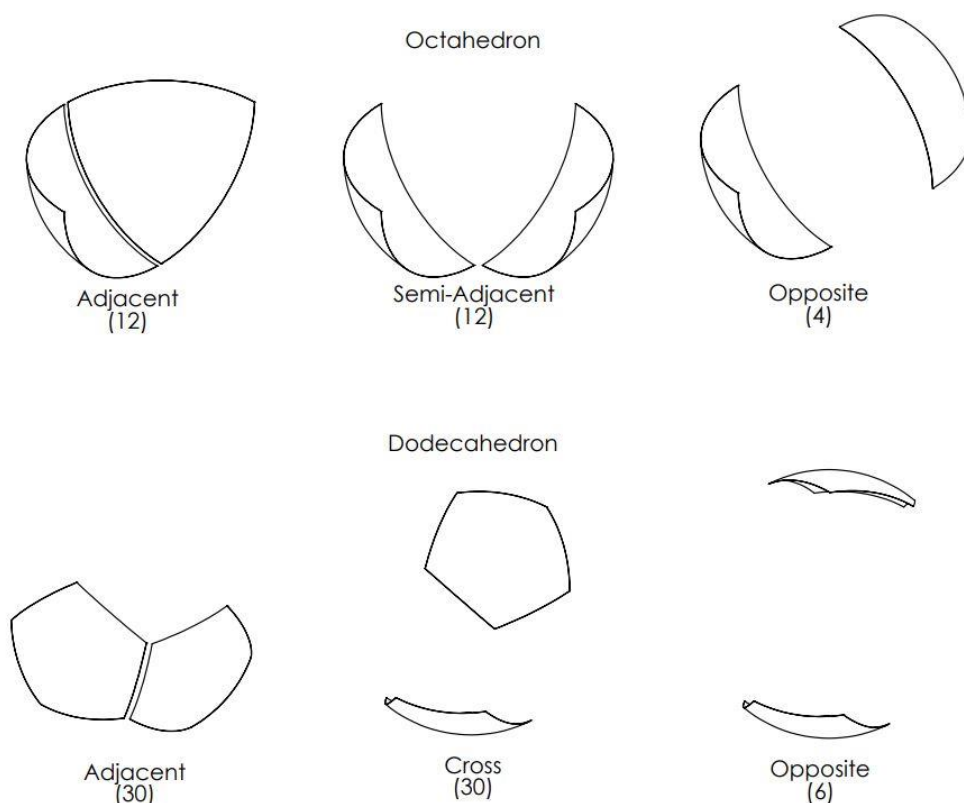


Figure 6: Channel Types

5. Results and Discussion

The Octahedron stratified fill data for all 28 channels is presented in Figure 7, organized by channel type. Figure 8 presents the average response of channel types. The opposite channels and most of the semi-adjacent channels have a similar fill curve shape. The magnitude increases linearly with fill level until it approaches the equator. Then, as a result of the singularities at the equator, has a large increase in signal as it passes through. As filling continues, there is almost no change in response from 0.6 to 1. The adjacent channels overall have an erratic response. Adjacent channels on the bottom of the hemisphere peak at a mass fraction around 0.5, well above the full normalization value, then decrease as filling continues. Adjacent channels in the top hemisphere have very little signal change until a mass fraction

of 0.5 where they then increase dramatically. When the test is repeated at 45° in Figure 9 and Figure 10, similar results are observed. Adjacent plates at the bottom have sharp increases in capacitance at low mass fractions. Adjacent channels also peak as they become submerged and then decrease in magnitude as filling continues. Opposite and semi-adjacent channels have a smoother curve because the singularities are more distributed and do not contact the fluid level all at once. When comparing Figure 8 and Figure 10, it is clear that there is low resolution between mass fractions of 0.6 and 1 and high uncertainty between mass fraction of 0 and 0.6 as fluid position changes.

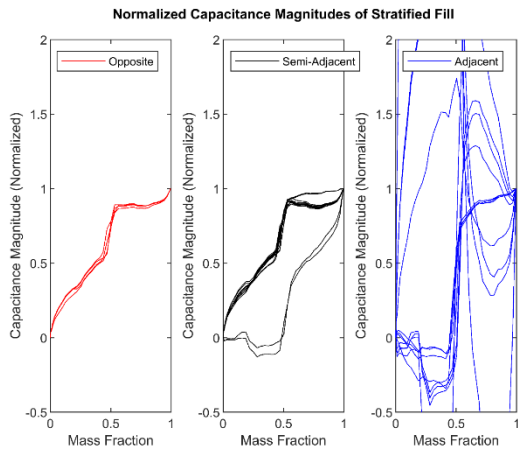


Figure 7: Octahedron Stratified Fill Data: All Channels

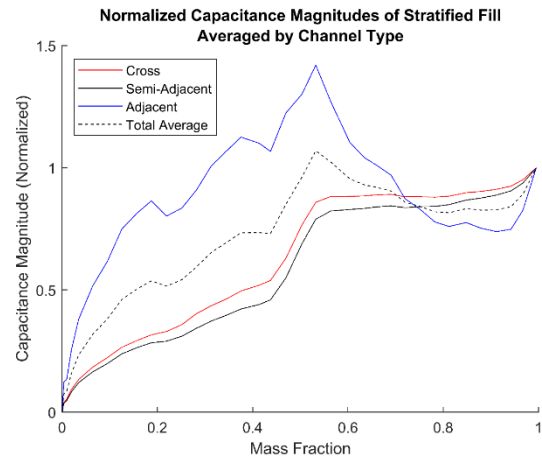


Figure 8: Octahedron Stratified Fill Data: Averaged by Channel Type

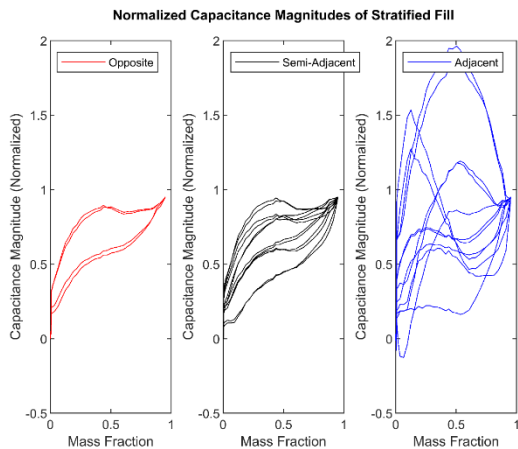


Figure 9: Octahedron 45° Fill: All Channels

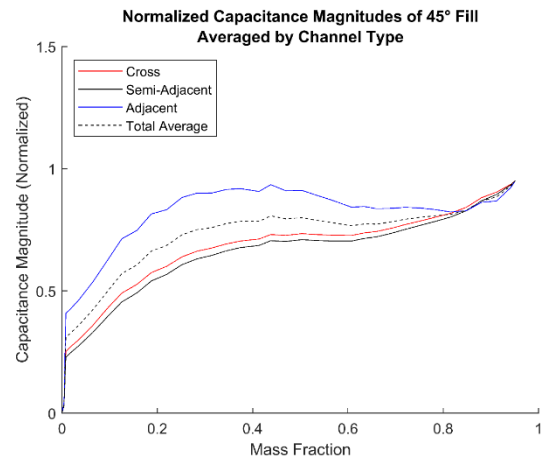


Figure 10: Octahedron 45° Fill: Averaged by Channel Type

Next the effect of the ball position is measured, by advancing the mass $\frac{1}{4}$ " at a time through the sensing region. In order to insert the ball apparatus into the sensing region, the sensor had to be disassembled and re-assembled. Small physical changes cause relatively large shifts in the normalization values, and due to the presence of the ball, the sensor cannot be normalized conventionally. For this test, the data was zeroed to the initial value and scaled based on the dynamic range of the stratified fill test. Based on this normalization method, a y-axis value of 1 represents a change equivalent to 100% of the dynamic range. In Figure 11 the responses are broken up by channel. The Opposite and Semi-Adjacent Channels have a shift of nearly the entire dynamic range, and the adjacent channels well exceed the dynamic range of the sensor. This data is averaged by channel type in Figure 12, demonstrating the poor overall

performance, even if adjacent channels are discarded. This is mainly due to the low dynamic range and low SNR of the sensor, allowing small noise and position changes to dramatically affect the overall measurement.

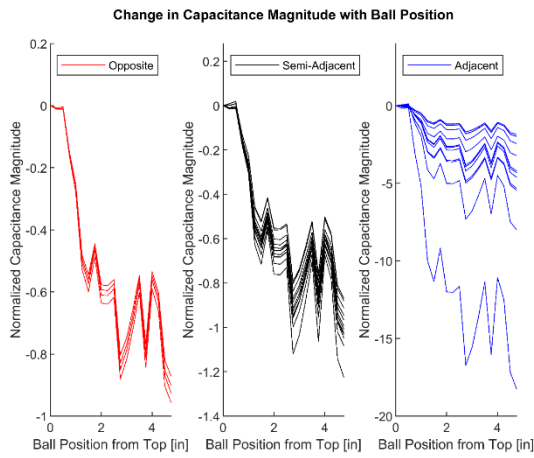


Figure 11: Octahedron Position Test: All Channels

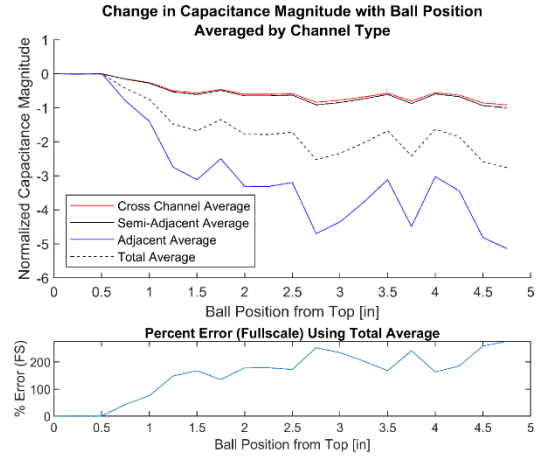


Figure 12: Octahedron Position Test: Averaged by Channel Type

The dodecahedron stratified fill data is presented in Figure 13 and Figure 14. Compared to the octahedron, the average dodecahedron response is highly linear with only small discontinuities at the poles. The difference in response to the 45° fill in Figure 15 and Figure 16 is distinguishable as the position of the singularities changes but is not nearly as substantial as the octahedron.

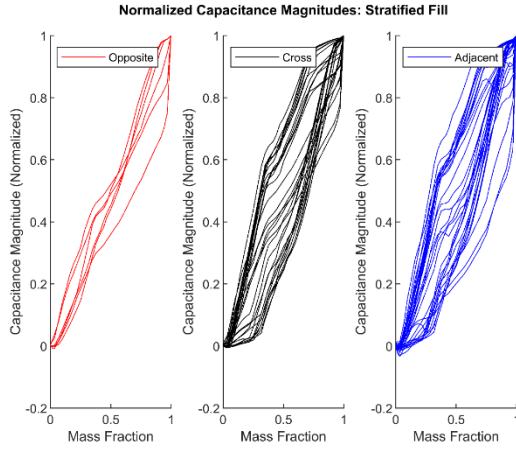


Figure 13: Dodecahedron Stratified Fill: All Channels

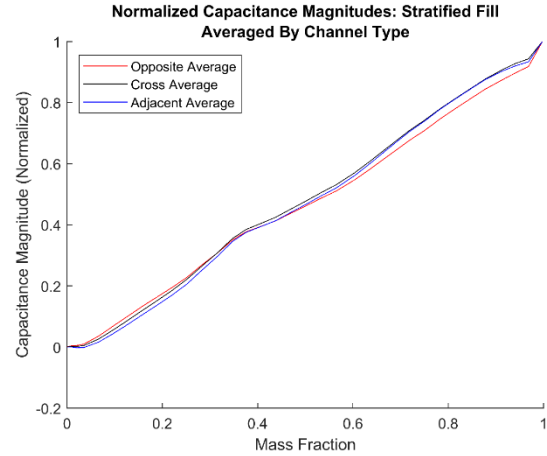


Figure 14: Dodecahedron Stratified Fill: Averaged by Channel Type

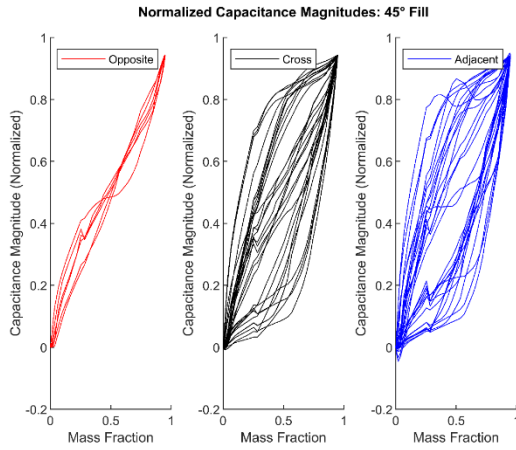


Figure 15: Dodecahedron 45° Fill: All Channels

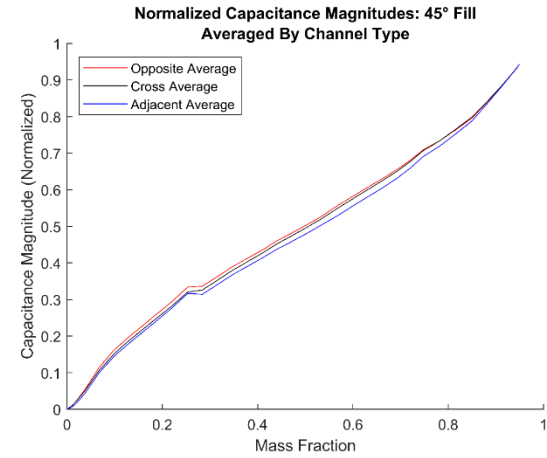


Figure 16: Dodecahedron 45° Fill: Averaged by Channel Type

The ball position test is conducted using the same method as the octahedron sensor, with the results presented in Figure 17 and Figure 18. Small signal changes are observed as the ball changes position, but due to the high dynamic range of this sensor design, they have a low effect on the overall signal, with a maximum error of 0.75%.

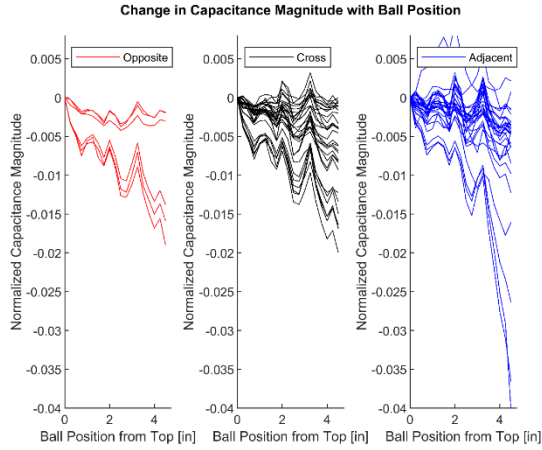


Figure 17: Dodecahedron Position Test: All Channels

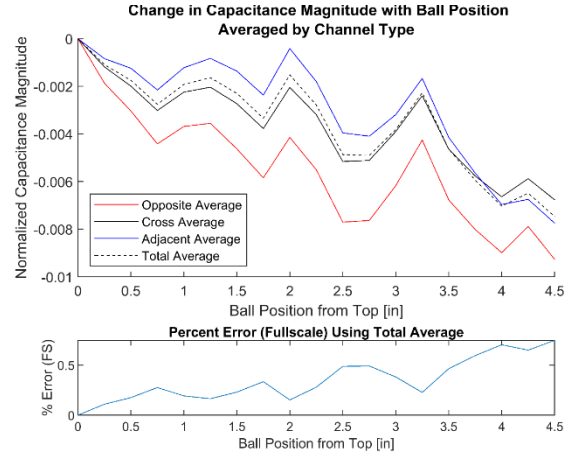


Figure 18: Dodecahedron Position Test: Averaged by Channel Type

	Dynamic Range				SNR [dB]			
	Opposite	Semi-Adjacent/Cross	Adjacent	Total Average	Opposite	Semi-Adjacent/Cross	Adjacent	Total Average
Octahedron	223.13	192.02	54.58	137.56	23.16	26.35	14.83	21.38
Dodecahedron	3056.31	3302.26	2956.66	3126.33	55.45	56.8	55.33	56.02

Table 4: Dynamic Range and SNR of Designs

The increase in linearity is a significant advantage of the dodecahedron design, but it is also accompanied by a large increase in Dynamic Range and SNR as shown in Table 4. These three factors make the design more sensitive, more robust, and more independent of fluid configuration.

The ECVT data can be analyzed through an averaging approach, where normalized capacitance magnitudes are averaged together or the data can be analyzed through an imaging approach, where a sensitivity matrix is used to inverse-solve an image of the fluid position in 3D space. The voxel density is then summed to create a volume fraction reading. ECVT image reconstruction is an inverse problem, where a large array of voxels, in this case 20x20x20, is reconstructed from a much smaller number of independent measurements. Using Equation 1, the Octahedron sensor has 28 independent channels, and the Dodecahedron has 66. The large discrepancy of independent measurements to reconstructed voxels results in an ill-posed reconstruction problem. A variety of reconstruction algorithms exist to address this complex inverse problem [22]. Many of these reconstruction methods, however, require information about the expected state and position of the fluid, and the image reconstruction error may vary when considering various arbitrary fluid configurations.

The simple averaging approach is calculated as follows. First the Adjacent channels are discarded. The Adjacent channels are sensitive to only a small fraction of the tank volume, have a high rotational instability, and in some cases a decreasing response as fill increases. Then the capacitance magnitudes for the stratified fill and 45° fill are fit with a 3rd order polynomial, heavily weighted at the endpoints. A percent \pm error due to fluid rotation can be generated by taking the maximum difference between the two fill profiles and the polynomial fit. It should be noted that this fit covers only 2 fill profiles, and due to the uneven sensitivity inside the sphere, ideally, all extreme fill types should be accounted for to

provide a better estimated error. An annular fill from the outside towards the center of the sphere, a ball fill from the center towards the radius, and a variety of unique angular stratified fills would cover the most extreme cases and provide a better error calculation.

The Octahedron fill profile is presented in Figure 19. A best-fit polynomial is generated for the two fill cases with the capacitance signal as the input and the mass fraction as the output. Provided the polynomial is monotonic, it could also be used as a calibration curve for the sensors to relate the volume fraction capacitance reading to the actual mass fraction. The instrument error with fluid rotation is the maximum difference at a given capacitance magnitude in indicated mass from real mass. Due to the large effect of the singularities in the octahedron design there is around 20% error between 0 and 50% fill, which slowly tapers down towards 100% fill. Because traditional tank gauging has high accuracy at high fill levels, this design presents no advantages.

The Dodecahedron profile in Figure 20 has a dramatically lower error. The more limited effect of singularities is seen as the curves diverge between 0 and 30% fill but the error decreases at higher fills. The maximum error for this design is around 5%, making a simple averaging approach suitable for unsettled medium accuracy applications, and the higher accuracy above 30% fill would be useful for leak detection in long voyages where settling thrust is unavailable [7].

An explanation for the differing effects of singularities can be found in Figure 21. During the stratified fill case, the octahedron encounters the majority of singularities all at once, at 50% fill. The 45° fill case more smoothly distributes the effect of the singularities, but the small dynamic range and the low symmetry of the design lead to wide discrepancies in fill curve profiles. The Dodecahedron on the other hand, encounters 15% of singularities at 4.5% fill and 30% of singularities at 26% fill. There is still curve

divergence but due to the greater dispersion of singularities, higher symmetry, and higher dynamic range the overall effect on the signal is greatly diminished.

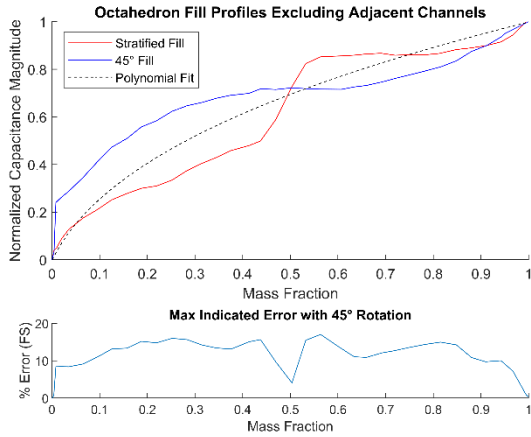


Figure 19: Octahedron Averaging Volume Fraction

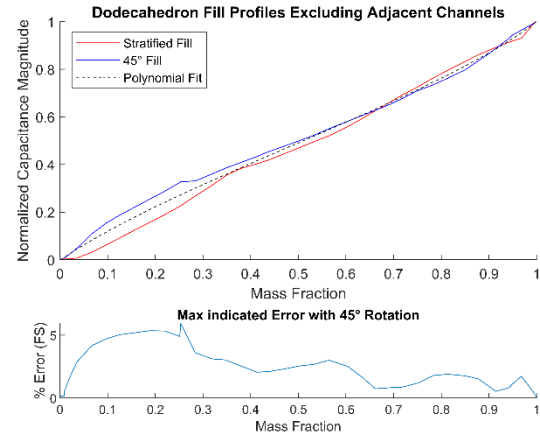


Figure 20: Dodecahedron Averaging Volume Fraction

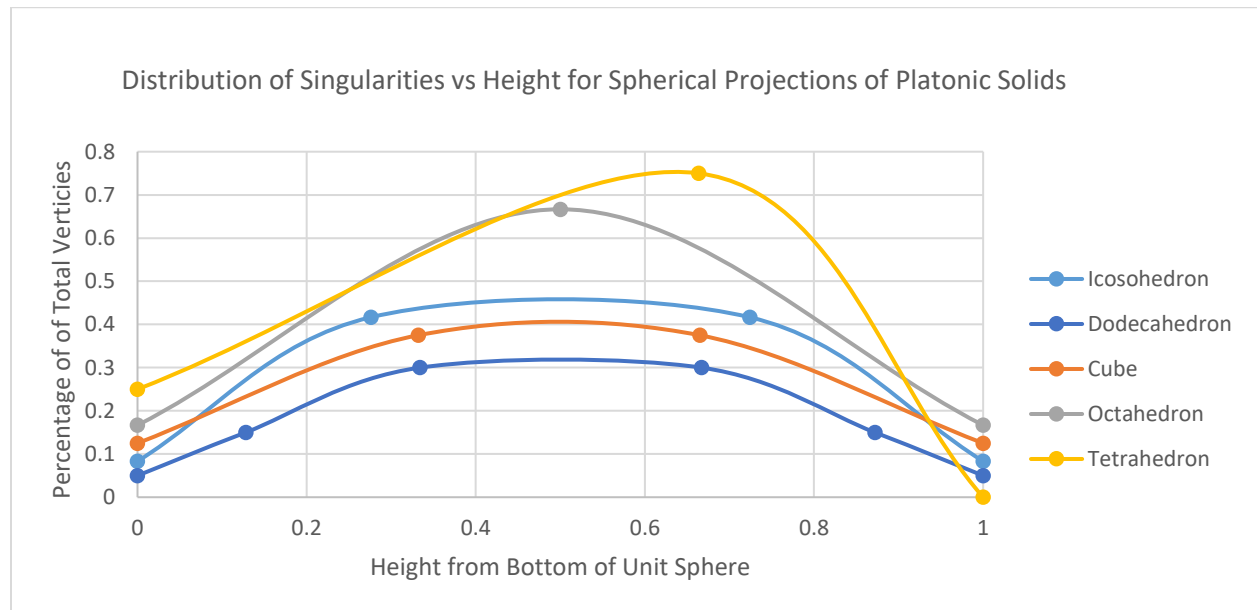


Figure 21: Singularity Distribution for Stratified Fills

Alternatively, the volume fraction is calculated using the ECVT imaging approach. Two different algorithms are used to generate the images, Linear Back Projection and Neural Network Multicriteria Optimization Reconstruction Technique (NNMOIRT) [18]. Once the image is generated as a 20x20x20 voxel array, the mean voxel value is taken as the volume fraction. The NNMOIRT alpha parameter was set to 5. LBP and NNMOIRT volume fractions for the octahedron sensor are plotted in Figure 22 and Figure 23 and for the dodecahedron in Figure 24 and Figure 25. It is important to note that the error in these figures is the error due to fluid rotation only. In Figure 23, the imaging volume fraction response to increasing fluid mass levels out and therefore, the overall error including noise would be very high above 30% mass fraction.

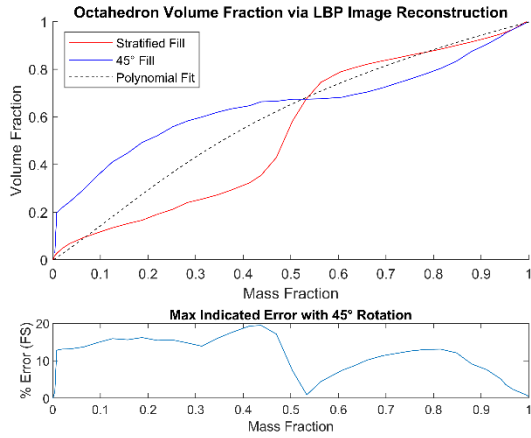


Figure 22: Octahedron LBP Volume Fraction

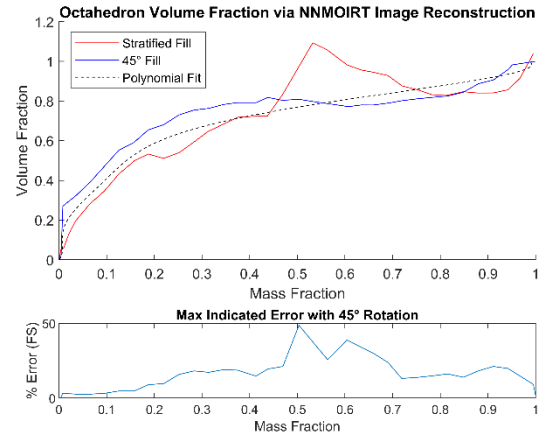


Figure 23: Octahedron NNMOIRT Volume Fraction

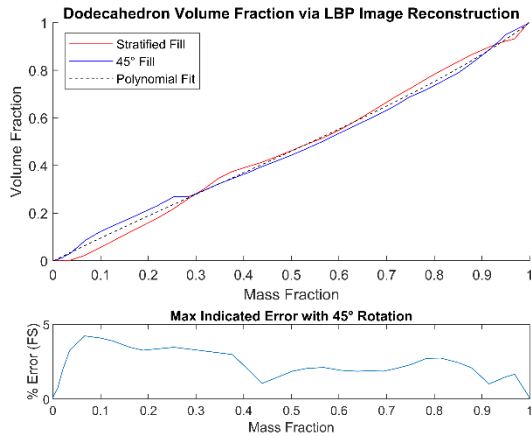


Figure 24: Dodecahedron LBP Volume Fraction

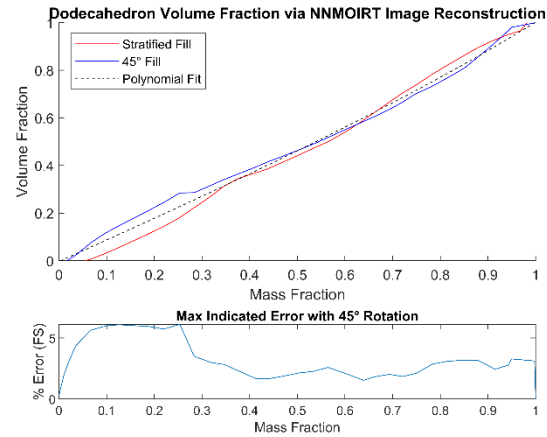


Figure 25: Dodecahedron NNMOIRT Volume Fraction

The 3D image reconstructions for selected volume fractions are shown in Figure 26 for reference. In each of these cases the stratified fill data is used to generate an image, but a stratified fluid boundary is not visible in the reconstructed image. Because of the limited number of electrodes clear images are not expected. Further increasing the number of plates would increase the accuracy of the reconstructed images but would not necessarily improve the volume fraction calculation as creating a clear image of the fluid configuration and accurately measuring the mass are two different considerations that would require differently optimized sensors. Table 5 lists the accuracy of the different volume fraction calculation methods. The Dodecahedron has dramatically improved accuracy values over the Octahedron. In all cases LBP and averaging are similar, with NNMOIRT having a higher max error. For the Octahedron, the averaging approach actually has better accuracy than the imaging, and for the Dodecahedron it is slightly worse than LBP.

Table 5: Accuracy of Volume Fraction Calculation Methods

		Averaging	LBP	NNMOIRT
Octahedron	Max Error	17.02 %	19.44 %	48.66 %
	Mean Error	8.37 %	7.90 %	10.11 %
Dodecahedron	Max Error	5.94 %	4.22 %	6.14 %
	Mean Error	1.96 %	1.59 %	2.40 %

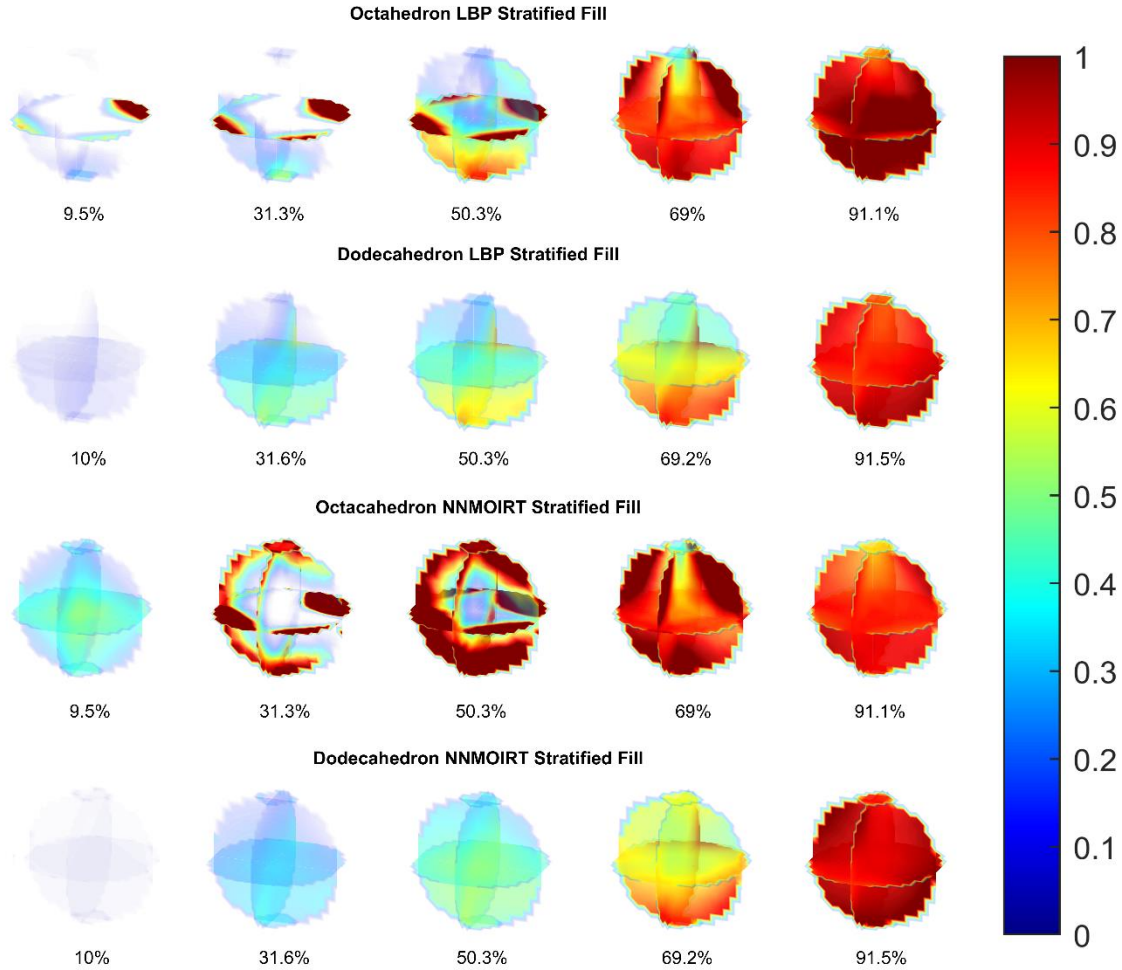


Figure 26: Image Reconstructions for Selected Volume Fractions

6. Conclusion

A well-performing ECVT mass gauge must have a high dynamic range and SNR, good signal linearity with respect to volume fraction, and high stability when fluid is moving inside the region. In the various tests discussed here, the dodecahedron sensor performed significantly better than the octahedron design. with around 5% error when the fluid is rotated 45° compared to the greater than 20% error of the octahedron. The Improvements to the Dynamic range, SNR, and Signal Linearity are primarily attributed the increase in the number of non-adjacent plates. The opposite channel performance of the

octahedron sensor was lower than expected, but this may be attributable to the large degree of curvature of the plates and the sharpness of the corners, concentrating sensitivity near the edges. The increase in rotational stability is attributed to the higher rotational order of the design, diminishing the effect of singularities on the response. The design complexity for each sensor is minimal but the dodecahedron is more complex to assemble due to the lack of a clear equator. The imaging resolution is better for the dodecahedron, but this effect is not observed in the collected data. The imaging approaches have very little advantage over averaging for the cases studied here when considering the volume fraction accuracy. It is possible that in microgravity, the surface tension dominated annular fluid configurations would be more accurately measured using an imaging approach, but the generated images in Figure 26 demonstrate that for both designs, the number of electrodes is insufficient to definitively determine the fluid configuration. The poor image reconstruction of the NNMOIRT approach suggests that the technique could be better optimized for this specific sensor geometry, but that investigation is outside the scope of this study.

The dodecahedron has slightly higher error at lower mass fractions but is still accurate enough that it would be a beneficial addition to traditional gauging methods that lose accuracy as fill level decreases. Furthermore, a combination of ECVT gauging in unsettled conditions with high accuracy level sensing methods for settled conditions, would provide additional propellant measurement during coasting and enable leak detection during long voyages, while maintaining high accuracy during thrust maneuvers.

7. Further Study

Further optimization of spherical ECVT mass gauges requires further study. Testing with microgravity fluid configurations is difficult on earth but would provide better calculations of error due to fluid configuration. This testing would also provide more insight into the relative advantage of less computationally intensive averaging-based approaches compared to image-based reconstruction algorithms. More sophisticated averaging algorithms that weigh the channel types according to their relative sensitivity may provide an accurate and fast volume fraction measurement method. Physics simulations of various fluid configurations are planned to further study these effects and the effect of propellant management devices.

For tank mass gauging, spherical tessellations provide the highest 3-dimensional symmetry, even in non-spherical volumes. Further study is needed on these non-spherical volumes. Projecting a spherical tessellation from the centroid of a volume, such as a cylinder, would create larger plates further from the centroid, increasing the homogeneity and potentially improving performance.

As the diameter of a tank increases it may be beneficial to switch to larger plates to maintain SNR. Further study regarding the effect of diameter on the optimal spherical sensor design is needed, as well as more detailed information on the performance of cube style and icosahedron style sensors to compare them with the results presented here. Further work is also needed to physically install and characterize the performance of these sensors in cryogenic and flight environments, but immediate applications of this technology could include mass gauging of fuel and oil tanks during aircraft flight or other dynamic conditions.

References

- [1] F. T. Dodge, "Propellant Mass Gauging: Database of Vehicle Applications and Research and Development Studies," NASA, 2008.
- [2] R. Balasubramaniam, E. Ramé and B. J. Motil, "Microgravity Liquid-Gas Two-Phase Flow: Review of Pressure Drop and Heat Transfer Correlations and Guidelines for Equipment Operability," National Aeronautics and Space Administration, Cleveland, 2019.
- [3] B. Yendler, "Review of Propellant Gauging Methods," in *44th AIAA Aerospace Sciences Meeting and Exhibit*, Reno, Nevada, 2006.
- [4] G. A. Zimmerli, K. R. Vaden, M. D. Herlacher, D. A. Buchanan and N. T. Van Dresar, "Radio Frequency Mass Gauging of Propellants," NASA/TM-2007-214907, Cleveland, 2007.
- [5] K. M. Crosby, R. J. Werlink and E. A. Hurlbert, "Liquid Propellant Mass Measurement in Microgravity," *Gravitational and Space Research*, no. 4, pp. 50-61, 2021.
- [6] National Aeronautics and Space Administration, "2020 NASA Technology Taxonomy," National Aeronautics and Space Administration, 2020.
- [7] G. A. Zimmerli, "Propellant Gauging for Exploration," in *54th JANNAF*, Denver, CO, 2017.
- [8] W. Yang, "Design of Electrical Capacitance Tomography Sensors," *Measurement Science and Technology*, vol. 21, no. 4, 2010.
- [9] S. M. Chowdhury, Q. M. Marashdeh, F. L. Teixeira and L.-S. Fan, "Electrical Capacitance Tomography," in *Industrial Tomography 2nd Edition*, Cambridge, Elsevier, 2022, pp. 3-29.
- [10] F. Wang, Q. Marashdeh, L.-S. Fan and W. Warsito, "Electrical Capacitance Volume Tomography: Design and Applications," *Sensors*, pp. 1890-1917, 2010.
- [11] A. Wang, "Electrical Capacitance Volume Tomography and its Applications in Multiphase Flow Systems," Columbus, OH, 2015.
- [12] S. H. Yang, Y. S. Kim, N. G. Dagalakos and Y. Wang, "Flexible Assemblies of Electrocapacitive Volume Tomographic Sensors for Gauging Fuel of Spacecraft," *Journal of Spacecraft and Rockets*, vol. 58, no. 2, 2021.
- [13] Z. Gut, "Using Electrical Capacitance Tomography System for Determination of Liquids in Rocket and Satellite Tanks," *Transactions on Aerospace Research*, vol. 1, pp. 18-33, 2020.
- [14] A. Wang, Q. Marashdeh and L.-S. Fan, "ECVT Imaging and Model Analysis of the Liquid Distribution inside a Horizontally Installed Passive Cyclonic Gas-Liquid Separator," *Chemical Engineering Science*, vol. 141, pp. 231-239, 2016.

- [15] S. M. Chowdhury, M. A. Charleston, Q. M. Marashdeh and F. L. Teixeira, "Propellant Mass Gauging in a Spherical Tank under Micro-Gravity Conditions Using Capacitance Plate Arrays and Machine Learning," *Sensors*, vol. 23, no. 20, 2023.
- [16] P. Behruzi, A. Hunt and R. Foster-Turner, "Evaluation of Liquid Sloshing using Electrical Capacitance Tomography," in *AIAA Propulsion and Energy Forum*, VIRTUAL EVENT, 2020.
- [17] A. Wang, Q. M. Marashdeh, F. L. Teixeira and L.-S. Fan, "Electrical Capacitance Volume Tomography: A Comparison between 12 and 24 Channels Sensor Systems," *Progress in Electromagnetics Research M*, vol. 41, pp. 73-84, 2015.
- [18] W. Warsito, Q. Marashdeh and L.-S. Fan, "Electrical Capacitance Volume Tomography," *IEEE Sensors Journal*, vol. 7, no. 4, pp. 525-535, 2007.
- [19] M. Atiyah and P. Sutcliffe, "Polyhedra in Physics, Chemistry and Geometry," *Milan Journal of Mathematics*, vol. 71, 2003.
- [20] D. R. Lide, CRC Handbook of Chemistry and Physics 73rd Edition, Boca Raton, Florida: CRC Press, Inc., 1992-1993.
- [21] Solvay Specialty Polymers, *Galden HT PFPE Heat Transfer Fluids*, 2013.
- [22] R. K. Rasel, S. M. Chowdhury, Q. M. Marashdeh and F. L. Teixeira, "Review of Selected Advances in Electrical Capacitance Volume Tomography for Multiphase Flow Monitoring," *Energies*, vol. 15, p. 5285, 2022.